Article:
Gade, A., Tostevin, J. A., Bader, V. et al. (13 more authors) (2016) Single-particle structure at N=29:The structure of Ar 47 and first spectroscopy of S 45. Physical Review C. 054315. ISSN 2469-9993

https://doi.org/10.1103/PhysRevC.93.054315

Single-particle structure at $N = 29$: The structure of ^{47}Ar and first spectroscopy of ^{45}S

A. Gade,[1,2] J. A. Tostevin,[3] V. Bader,[1,2] T. Baugher,[1,2] D. Bazin,[1] J. S. Berryman,[1] B. A. Brown,[1,2] C. Aa. Diget,[1,*] T. Glasmacher,[1,2] D. J. Hartley,[4] E. Lunderberg,[1,2] S. R. Stroberg,[1,2,†] F. Recchia,[1] A. Ratkiewicz,[1,2,‡] D. Weisshaar,[1] and K. Wimmer[5,1,§]

[1]*National Superconducting Cyclotron Laboratory, Michigan State University, East Lansing, Michigan 48824, USA*
[2]*Department of Physics and Astronomy, Michigan State University, East Lansing, Michigan 48824, USA*
[3]*Department of Physics, University of Surrey, Guildford, Surrey GU2 7XH, United Kingdom*
[4]*Department of Physics, U.S. Naval Academy, Annapolis, Maryland 21402, USA*
[5]*Department of Physics, Central Michigan University, Mount Pleasant, Michigan 48859, USA*

(Dated: April 22, 2016)

Comprehensive spectroscopy of the $N = 29$ nucleus ^{47}Ar is presented, based on two complementary direct reaction mechanisms: one-neutron pickup onto ^{46}Ar projectiles and one-proton removal from the 1^- ground state of ^{48}K. The results are compared to shell-model calculations that use the state-of-the-art SDPF-U and SDPF-MU effective interactions. Also, from the ^{9}Be(^{46}Cl,^{45}S+γ)X one-proton removal reaction, we report the first γ-ray transitions observed from ^{45}S. Using comparisons with shell-model calculations, and from the observed intensities and energy sums, we propose a first tentative level scheme for ^{45}S.

I. INTRODUCTION

The region around the neutron-rich $N = 28$ isotones ^{46}Ar, ^{44}S and ^{42}Si has provided much insight into the changes to nuclear structure that occur in neutron-rich nuclei. First evidence for a breakdown of the $N = 28$ magic number in ^{44}S, from an emergence of collectivity, was hinted at by β-decay work [1] and was ultimately quantified with intermediate-energy Coulomb excitation [2, 3]. More recently, shape- and configuration-coexistence was established in ^{44}S [4–7], adding to the rich structure observed at neutron number $N = 28$ in the sulfur isotopes. Beyond $N = 28$, only the energy of the first excited 2^+ state in ^{46}S has been reported [8]. Two protons below, in ^{42}Si, excitations (of quadrupole nature) across the reduced $N = 28$ and $Z = 14$ sub-shell gaps mutually enhance one another, contributing to deformation and making ^{42}Si the most collective nucleus in the region [9, 10]. No spectroscopic information is available beyond $N = 28$ in the silicon isotopes. Shell-model calculations in the *sd-pf* shell, using the SDPF-U [11] and SDPF-MU [10] effective interactions, have been very successful in describing the available experimental observations for ^{44}S [4, 5] and ^{42}Si [9, 12], which are related to collectivity and shape.

The less-neutron-rich ^{46}Ar system, located between doubly-magic ^{48}Ca and collective ^{44}S on the nuclear chart, has challenged the existing shell-model (SM) descriptions. While some observables, for example those related to the masses of the Ar isotopes around $N = 28$ [13], are well described, calculations appear to over-predict the $B(E2)$ excitation strength to the first 2^+ state [2, 14–16]. This result is not without controversy, on the experimental side, where an excited-state lifetime measurement yields higher collectivity, in agreement with the shell model [17], but is at odds with several Coulomb excitation measurements that consistently yield a lower $B(E2)$ value [2, 14, 16]. Using an inverse kinematics ^{46}Ar(d, p) reaction, states in ^{47}Ar with significant single-neutron spectroscopic strength were measured [18] and were used in the development of the SDPF-U SM effective interaction [11]. Beyond $N = 28$, $B(E2)$ transition strengths were measured for ^{47,48}Ar [15], and γ-ray spectroscopy following deep-inelastic reactions [19] and nucleon exchange [8] were performed for ^{47,48}Ar and ^{48}Ar, respectively. Most recently, excited states of ^{50}Ar were populated for the first time in secondary fragmentation reactions [20].

Here we present a new study of ^{47}Ar using two complementary intermediate-energy direct nuclear reactions: (i) the neutron-adding ^{12}C(^{46}Ar,^{47}Ar+γ)X reaction, and (ii) the ^{9}Be(^{48}K,^{47}Ar+γ)X proton removal reaction. We also report the first spectroscopy of ^{45}S, populated in the one-proton removal reaction from ^{46}Cl projectiles.

II. THEORETICAL DESCRIPTION

As the selectivity seen in the measurements and the interpretation of results are closely tied to the reaction mechanism and the nuclear structure, we first discuss the theory. The interpretation of the data reported here combines nuclear shell-model and reaction model calculations. In the following subsections, we discuss and summarize the parameters relevant to these theoretical inputs.

*Present address: Department of Physics, University of York, Heslington, York YO10 5DD, United Kingdom
†Present address: TRIUMF, Vancouver, British Columbia V6T 2A3, Canada
‡Present address: Lawrence Livermore National Laboratory, Livermore, California 94551, USA
§Present address: Department of Physics, The University of Tokyo, Hongo, Bunkyo-ku, Tokyo 113-0033, Japan

A. Shell model calculations

We employ shell-model calculations made with the SDPF-U [11] and the more recent SDPF-MU [10] effective Hamiltonians. These Hamiltonians were designed to be used in a model space with the full set of configurations made from protons in the $(2s_{1/2},1d_{5/2},1d_{3/2})$ (sd) set of orbitals and neutrons in the $(2p_{3/2},2p_{1/2},1f_{7/2},1f_{5/2})$ (pf) set of orbitals. The calculations were carried out with the code NuShellX [21]. The former (SDPF-U), tuned for $0\hbar\omega$-truncated pf-shell calculations of neutron-rich silicon isotopes, incorporated theoretical and empirical information that enhanced reliability for these isotopes. The latter (SDPF-MU) theoretical study incorporated and clarified the importance of including tensor-force components in the *sd-pf* cross-shell proton-neutron interaction for reproducing the measured 2_1^+- and 4_1^+-state energies and the $B(E2,0^+\rightarrow 2^+)$ values in the silicon and sulfur isotopes near $N\approx 28$ – including the energy of the (tentatively) assigned ^{42}Si 4_1^+ state in Ref. [22]. Wave functions and spectroscopic factors, C^2S, are computed for both interactions and all final states below the one-neutron emission thresholds of the ^{47}Ar and ^{45}S residual nuclei.

B. Reaction model calculations

1. Proton-removal calculations

The use of the nucleon-removal reaction technique for the spectroscopy of nuclei produced as fast secondary beams is now well established [23], exploiting both their high detection efficiency and sizeable cross sections. The key approximations made, of eikonal dynamics and spectator cores, were recently summarized in Ref. [24]. We first detail the parameters used in the proton-removal calculations from ^{48}K. A ^{9}Be reaction target was used at an incident beam energy (at mid-target) of 87.5 MeV/u. Here, $J^\pi_{i,f}$ will label the spins and parities of the ^{48}K projectile ground state (i) and of the ^{47}Ar residue states (f). The active single-particle orbitals, $\alpha\equiv[n\ell j]$, from which the proton is removed are denoted ψ_α. The model inputs use the systematic approach detailed in Section III of Ref. [25]. The geometries of the complex residue- and proton-target distorting potentials are deduced from the neutron and proton densities of ^{47}Ar and the ^{9}Be target density. The ^{47}Ar-target interaction is calculated using the double-folding ($t_{NN}\rho_c\rho_t$) model with an effective nucleon-nucleon (NN) interaction t_{NN}. The proton-target interaction is calculated using the single-folding ($t_{NN}\rho_t$) model. The ^{47}Ar density (ρ_c) is taken from a spherical Skyrme (SkX interaction [26]) Hartree-Fock (HF) calculation. A Gaussian density (ρ_t) with rms radius of 2.36 fm is assumed for ^{9}Be. t_{NN} is also assumed to be Gaussian [27] with a range parameter 0.5 fm. Its (complex) strength was determined from: (a) the free NN cross sections, and (b) the ratio of the real-to-imaginary parts of the forward scattering NN amplitude for 100 MeV/u, as tabulated by Ray [28].

The geometries of the Woods-Saxon (WS) potentials that bind the removed protons are deduced from the root mean squared (rms) radii of the active proton orbitals from HF calculations for ^{48}K. These WS potentials have a fixed diffuseness $a_0=0.7$ fm and spin-orbit strength $V_{\rm so}=6$ MeV. The deduced radius parameters, r_0, were 1.287, 1.325, and 1.324 fm for the $2s_{1/2}$, $1d_{3/2}$ and $1d_{5/2}$ orbitals, respectively. The WS potential depth for each ψ_α was adjusted to reproduce the physical separation energy for the removal reaction to each final state, i.e. $S_p^{fi}=S_p+E_f$, where S_p is the ground-state to ground-state proton separation energy of 14.362 MeV [29].

The same approach was used for the proton-removals from ^{46}Cl(J_i^π) where the incident beam energy (at mid-target) is 86.6 MeV/u. Here, the deduced $2s_{1/2}$, $1d_{3/2}$ and $1d_{5/2}$ bound states radius parameters r_0 are 1.292, 1.332, and 1.323 fm, and the ground-state to ground-state proton separation energy is 17.10 MeV [29].

Table I shows the details of the calculated single-particle cross sections for ^{48}K (with $C^2S=1$, and denoted $\sigma_\alpha^{\rm sp}$), being the contributions from each ψ_α orbital to the given final state. Calculations using the C^2S of the ^{48}K(1_1^-) SDPF-U and the SDPF-MU SM wave functions are also shown. The SM level energies are used. In constructing the theoretical cross sections, the *sd*-shell SM C^2S are multiplied by the (near-unity) $[A/(A-1)]^2$ center-of-mass correction. We show the theoretical cross sections for each α, $\sigma_\alpha^{\rm th}$, and for each final state, $\sigma^{\rm th}(J_f^\pi)$, the sums of the α contributions. All energies are in MeV and all cross sections are in mb. We have assumed here the 1^- ground-state spin assignment of ^{48}K [30].

Table II collects a summary of these ^{48}K(1_1^-) to ^{47}Ar(J_f^π) partial cross sections for the SDPF-U and SDPF-MU SM wave functions. Also shown are the cross-section-weighted asymmetries, $\Delta S=S_p^{fi}-S_n$, of the effective proton and neutron separation energies from ^{48}K, for which $S_n=4.644$ MeV [29].

The corresponding summary of partial cross sections for the proton removal reaction from ^{46}Cl(1^-), using both the SDPF-U and SDPF-MU SM wave functions, is presented in Table III. The neutron separation energy from ^{46}Cl, used in the cross-section-weighted asymmetry ΔS, is now $S_n=3.52$ MeV [29] (see Section III.B for a discussion on the ground-state spin of ^{46}Cl).

2. Neutron-pickup calculations

The ^{46}Ar$(^{12}$C$,^{11}$C$)^{47}$Ar neutron pickup calculations follow the distorted wave Born approximation (DWBA) approach discussed in Ref. [31] and its supplemental information [32]. This approach produces the optimal theoretically and experimentally constrained data set used here. The neutron-pickups from ^{12}C are assumed to populate the $I^\pi=3/2_1^-$ (g.s.), $1/2_1^-$ (2.0 MeV), and

TABLE I: Calculated partial cross sections to ^{47}Ar(J_f^π) final states, with energy E_f, following proton removal from ^{48}K. The ^{48}K beam energy is 87.5 MeV/u on a ^{9}Be target. The calculations take the spectroscopic factors, C^2S, from SDPF-U and SDPF-MU interaction shell model calculations and assume the ^{48}K ground-state is the $J_i^\pi = 1_1^-$ shell model state. The shell model energies are used. The ^{48}K 1_1^- state for the SDPF-U and SDPF-MU shell model interactions lies at 395 and 262 keV, respectively. The theoretical cross sections include the $[A/(A-1)]^2$ center-of-mass correction for removals from the *sd*-shell.

J_i^π	J_f^π	ψ_α	E_f (MeV)	$\sigma_\alpha^{\rm sp}$ (mb)	C^2S (SDPF-U)	$\sigma_\alpha^{\rm th}$ (mb)	$\sigma^{\rm th}(J_f^\pi)$ (mb)	E_f (MeV)	$\sigma_\alpha^{\rm sp}$ (mb)	C^2S (SDPF-MU)	$\sigma_\alpha^{\rm th}$ (mb)	$\sigma^{\rm th}(J_f^\pi)$ (mb)
1_1^-	$3/2^-$	$2s_{1/2}$	0.000	10.15	0.1954	2.069	3.931	0.000	10.15	0.2446	2.590	4.328
		$1d_{3/2}$		7.95	0.2181	1.809			7.95	0.2016	1.672	
		$1d_{5/2}$		9.30	0.0055	0.053			9.30	0.0068	0.066	
1_1^-	$1/2^-$	$2s_{1/2}$	1.139	9.67	0.0014	0.014	0.367	0.931	9.76	0.0000	0.000	0.091
		$1d_{3/2}$		7.65	0.0443	0.353			7.70	0.0113	0.091	
1_1^-	$5/2^-$	$1d_{3/2}$	1.277	7.61	0.4037	3.205	3.655	1.139	7.65	0.4530	3.613	4.185
		$1d_{5/2}$		8.88	0.0486	0.450			8.92	0.0615	0.572	
1_1^-	$7/2^-$	$1d_{5/2}$	1.575	8.78	0.0428	0.392	0.392	1.371	8.85	0.0578	0.533	0.533
1_1^-	$3/2^-$	$2s_{1/2}$	2.125	9.29	0.2680	2.598	2.604	1.918	9.37	0.1073	1.049	1.202
		$1d_{3/2}$		7.41	0.0003	0.002			7.45	0.0192	0.149	
		$1d_{5/2}$		8.62	0.0004	0.004			8.68	0.0004	0.004	
1_1^-	$5/2^-$	$1d_{3/2}$	2.836	7.24	0.0404	0.305	0.522	2.379	7.35	0.0246	0.188	0.284
		$1d_{5/2}$		8.42	0.0247	0.217			8.54	0.0107	0.095	
1_1^-	$5/2^-$	$1d_{3/2}$	3.384	7.12	0.0001	0.001	0.003	2.752	7.26	0.0144	0.109	0.124
		$1d_{5/2}$		8.27	0.0003	0.003			8.44	0.0017	0.015	
Incl.					1.29		11.47			1.21		10.75

TABLE II: Summary of the calculated ^{48}K(1^-) to ^{47}Ar(J_f^π) proton-removal partial cross sections using the SDPF-U and SDPF-MU shell-model wave functions, collected from Table I. The shell-model energies are used. The calculated partial cross-section-weighted asymmetries, $\Delta S = S_p^{fi} - S_n$, of the proton and neutron separation energies from ^{48}K are also shown.

SDPF-U ^{47}Ar(J_f^π)	E_f(U) (MeV)	$\sigma^{\rm th}$(U) (mb)	SDPF-MU ^{47}Ar(J_f^π)	E_f(MU) (MeV)	$\sigma^{\rm th}$(MU) (mb)
$3/2^-$	0.000	3.931	$3/2^-$	0.000	4.328
$1/2^-$	1.139	0.367	$1/2^-$	0.931	0.091
$5/2^-$	1.277	3.655	$5/2^-$	1.139	4.185
$7/2^-$	1.575	0.392	$7/2^-$	1.371	0.533
$3/2^-$	2.125	2.604	$3/2^-$	1.918	1.202
$5/2^-$	2.836	0.522	$5/2^-$	2.379	0.284
$5/2^-$	3.384	0.003	$5/2^-$	2.752	0.124
Incl. (mb)		11.47			10.75
ΔS (MeV)		10.83			10.55

TABLE III: Summary of the calculated proton-removal partial cross sections from ^{46}Cl(1^-) at 86.6 MeV/u, based on the SDPF-U and SDPF-MU shell-model wave functions. The shell-model energies are used. The calculated partial cross-section-weighted asymmetries, $\Delta S = S_p^{fi} - S_n$, of the proton and neutron separation energies from ^{46}Cl are also shown.

SDPF-U ^{45}S(J_f^π)	E_f(U) (MeV)	$\sigma^{\rm th}$(U) (mb)	SDPF-MU ^{45}S(J_f^π)	E_f(MU) (MeV)	$\sigma^{\rm th}$(MU) (mb)
$3/2^-$	0.000	2.848	$3/2^-$	0.000	3.425
$1/2^-$	0.633	1.588	$1/2^-$	0.239	0.589
$7/2^-$	0.746	0.138	$3/2^-$	0.941	0.778
$3/2^-$	1.098	0.449	$5/2^-$	1.109	2.702
$7/2^-$	1.394	0.244	$7/2^-$	1.148	0.379
$5/2^-$	1.473	0.650	$5/2^-$	1.421	0.103
$5/2^-$	2.045	0.188	$3/2^-$	1.680	0.889
$1/2^-$	2.079	0.592	$1/2^-$	2.001	0.173
$3/2^-$	2.101	0.963	$3/2^-$	2.156	0.252
$7/2^-$	2.161	0.030	–	–	–
Incl. (mb)		7.69			9.29
ΔS (MeV)		14.46			14.34

$3/2_2^-$ (4.8 MeV) bound final states of ^{11}C. For these ^{12}C neutron-removal vertices (overlaps) we use the extracted spectroscopic factors (SF) from the analyses of final-state-exclusive ^{12}C$(e,e'p)$ proton-removal measurements, as presented in Table 8 of Ref. [33], of 1.72(11), 0.26(2), and 0.20(2), respectively. In the present ^{47}Ar case, the reduced radii, r_0, from the (Hartree-Fock constrained) Woods-Saxon neutron potentials, that bind the $2p_{3/2}$, $2p_{1/2}$, $1f_{7/2}$ and $1f_{5/2}$ orbitals, are 1.069, 1.095, 1.211 and 1.221 fm, respectively. These potentials have

the same fixed diffuseness $a_0 = 0.7$ fm and spin-orbit interaction strength $V_{so} = 6.0$ MeV as in the removal calculations. A summary of the calculated cross sections to the SDPF-U and SDPF-MU ^{47}Ar(J_f^π) SM final states are presented in Table IV.

TABLE IV: Summary of the calculated partial cross sections for the ^{46}Ar(^{12}C, ^{11}C)^{47}Ar(J_f^π) neutron-pickup reaction at 62 MeV/u for those bound ^{47}Ar(J_f^π) final states with significant spectroscopic factors. The $\sigma^{\rm th}$(U) and $\sigma^{\rm th}$(MU), that use the SDPF-U and SDPF-MU SM wave functions and overlaps, are the sums of the yields to the $3/2_1^-$(g.s.), $1/2_1^-$(2.0 MeV), and $3/2_2^-$(4.8 MeV) ^{11}C final states. The shell model energies are used.

^{47}Ar	E_f (U)	C^2S	$\sigma^{\rm th}$(U)	E_f (MU)	C^2S	$\sigma^{\rm th}$(MU)
J_f^π	(MeV)	sdpf-u	(mb)	(MeV)	sdpf-mu	(mb)
$3/2^-$	0.000	0.711	0.017	0.000	0.634	0.016
$1/2^-$	1.139	0.834	0.004	0.931	0.861	0.005
$5/2^-$	1.277	0.011	0.007	1.139	0.032	0.021
$7/2^-$	1.575	0.071	0.108	1.371	0.092	0.142
$5/2^-$	2.836	0.182	0.104	2.379	0.235	0.140
$5/2^-$	3.384	0.440	0.235	2.753	0.331	0.190
Incl.	(mb)		0.476			0.513

III. EXPERIMENTS AND DISCUSSION

All measurements described in the present work were performed at the Coupled Cyclotron Facility at the National Superconducting Cyclotron Laboratory (NSCL) on the campus of Michigan State University.

The particle identification for all measurements was performed event-by-event with the focal-plane detection system of the large-acceptance S800 spectrograph [34]. The energy loss measured with the S800 ionization chamber and time-of-flight information, taken between plastic scintillators, corrected for the angle and momentum of each ion, were used to unambiguously identify the reaction residues emerging from the target. The particle-identification spectra for ^{47}Ar and ^{45}S from one-proton removal are shown in Fig. 1(a) and (b), as examples.

Gamma-ray detection was performed with SeGA [35] or GRETINA [36], set up around the target position of the S800 spectrograph. The photopeak efficiency of each array was calibrated with standard sources and corrected for the Lorentz boost of the γ-ray distribution emitted by the residual nuclei moving at more than 30% of the speed of light. The γ-ray intensities, corrected for the efficiency and indirect feeding, were used to derive the partial cross sections for the population of individual final states.

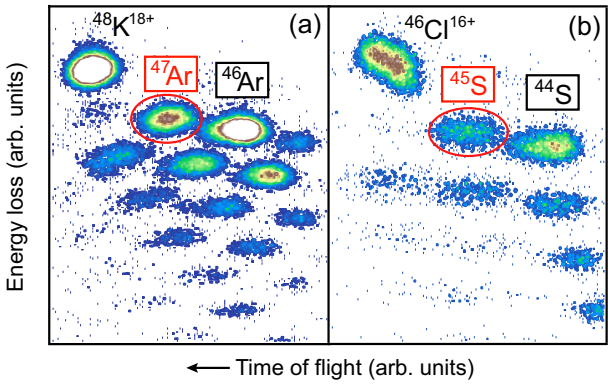

FIG. 1: (Color online) Particle identification spectra for the one-proton removal reactions to: (a) ^{47}Ar, and (b) ^{45}S, used to determine the inclusive cross sections. The most intense structure in each spectrum is the hydrogen-like charge state of the projectile beam.

A. ^{47}Ar populated in one-neutron pickup and one-proton removal

For the ^{12}C(^{46}Ar,^{47}Ar+γ)X one-neutron pickup reaction, the secondary beam of ^{46}Ar (100% pure) was produced from a 140 MeV/u stable ^{48}Ca primary beam interacting with a 1363 mg/cm^2 ^{9}Be production target in the A1900 fragment separator [37]. A 240 mg/cm^2 Al degrader was used for separation. A comparably thick production target was used to degrade the beam energy to 67 MeV/u to increase the pickup cross section (see the discussion in Ref. [31]). The total momentum acceptance of the A1900 was restricted to $\Delta p/p = 0.25\%$, resulting in an on-target rate of about 3×10^5 ^{46}Ar/s. A 149 mg/cm^2 glassy carbon target was used to induce the one-neutron pickup reaction. The high-resolution γ-ray detection system GRETINA [36], an array of 36-fold segmented high-purity Ge detectors, surrounded the target position and measured the prompt γ rays emitted by the reaction products. The seven GRETINA modules, with four crystals each, were arranged in two rings. Four modules were located at 58° center angle with respect to the beam axis and three modules occupied adjacent positions in the 90° ring. Online signal decomposition provided γ-ray interaction points for event-by-event Doppler reconstruction of the photons emitted in flight at 30% of the speed of light. The momentum vector of projectile-like reaction residues, as obtained from trajectory reconstruction through the S800 spectrograph, was incorporated into the Doppler reconstruction. The resulting γ-ray spectrum is shown in Fig. 2(a).

For clean particle identification, γ-ray coincidences were required to eliminate a tail of unreacted ^{46}Ar projectiles entering the focal plane. Due to this small projectile beam contamination, absolute partial cross sections could be cleanly extracted for the excited states, but only an upper limit can be deduced for the inclusive and ground state cross sections ($\sigma_{inc}^{+1n} \leq 0.48(3)$ mb).

As shown in Ref. [31], the spin alignment in fast-beam one-nucleon pickup is strong. Thus, because of its broad angular coverage, the γ-ray angular distributions have to be taken into account for a precise determination of the in-beam γ-ray efficiency of the GRETINA array. Here, for mixed $M1/E2$ transitions, we used the multipole mixing ratios δ from the SDPF-MU shell model calculations to determine the angular distributions and account for their effect on the in-beam γ-ray efficiency of GRETINA. A 10% systematic uncertainty was added to the intensities of transitions with mixed $M1/E2$ multipolarity to account for the uncertainty introduced by this choice. The statistics were not sufficient for an angular distribution analysis as presented in [31].

For the ^{9}Be(^{48}K,^{47}Ar+γ)X one-proton removal reaction, the secondary beam of ^{48}K (100% pure) was produced from a 140 MeV/u stable primary beam of ^{48}Ca impinging on a 705 mg/cm^2 ^{9}Be production target at the entrance of the A1900 fragment separator [37] and separated using a 390 mg/cm^2 Al degrader. The total momentum acceptance of the A1900 was restricted to $\Delta p/p = 0.5\%$, yielding a rate on target of 1.1×10^5 ^{48}K/s. The 376 mg/cm^2 thick ^{9}Be reaction target was surrounded by SeGA, an array of 32-fold segmented high-purity germanium detectors [35]. The high degree of segmentation enables event-by-event Doppler reconstruction of the energies of γ rays emitted in flight by the reaction residues. The emission angle needed for the Doppler reconstruction was determined from the position of the segment that registered the largest γ-ray energy deposition. The 16 detectors of SeGA were arranged in two rings with 90° and 37° central angles with respect to the beam axis. Seven detectors were located at 37°, while the 90° ring was equipped with nine detectors. The resulting γ-ray spectrum is shown in Fig. 2(b).

The inclusive cross section for the ^{9}Be(^{48}K,^{47}Ar)X one-proton removal reaction, of $\sigma_{inc}^{-1p} = 5.4(3)$ mb, was derived from the yield of ^{47}Ar reaction residues divided by the number of incoming ^{48}K projectiles relative to the number density of the reaction target. A systematic uncertainty of 5%, attributed to the stability of the incoming beam for normalization, has been added in quadrature to the statistical uncertainty. This inclusive cross section was determined in a dedicated run with ^{47}Ar centered in the S800 focal plane. The high-statistics setting for the measurement of partial cross sections is the one run in the measurement described in [8], with the low-momentum tail slightly cut, possibly introducing an ℓ-dependent uncertainty in the determination of the partial cross sections relative to the total number of ^{47}Ar. A conservative 10% systematic uncertainty was added in quadrature to the statistical uncertainty of the partial cross sections deduced from the γ-ray data.

The γ-ray spectra in Fig. 2(a) and (b) highlight the complementarity of the two direct reaction mechanisms used to populate excited states in ^{47}Ar, with rather different intensity patterns and the unique observation of some states in one of the reactions only. As is discussed in Ref. [31], the fast-beam-induced one-neutron pickup reaction selectively populates states with high orbital angular momenta; i.e. $\ell = 3$ in the case of the ^{12}C(^{46}Ar,^{47}Ar+γ)X reaction. States with $\ell = 4$ have been suggested above the neutron separation energy [18] but cannot be observed in the present work in the absence of γ-ray branches. The high coincidence efficiency of GRETINA allowed for the use of $\gamma\gamma$ coincidences to establish the level scheme. Such a coincidence spectrum is shown as inset to Fig. 2(a) where the 1231-keV transition was clearly found in coincidence with γ rays at 515 keV and 1017 keV. For ^{47}Ar produced in one-proton removal from ^{48}K, SeGA's coincidence efficiency and the statistics (in all lines but 1229(5) keV) are too low for $\gamma\gamma$ coincidence analyses. Based on $\gamma\gamma$ coincidences, where possible, and with the help of energy sums and previously reported energies [18], the level schemes shown in Fig. 3 were constructed. Both level schemes show all bound states of ^{47}Ar known so far; transitions and levels marked in black were observed in the respective setting. The only level that was not observed in either of our measurements is the proposed $1/2^-$ state at 1130 keV [18]. As we point out below, our non-observation of the

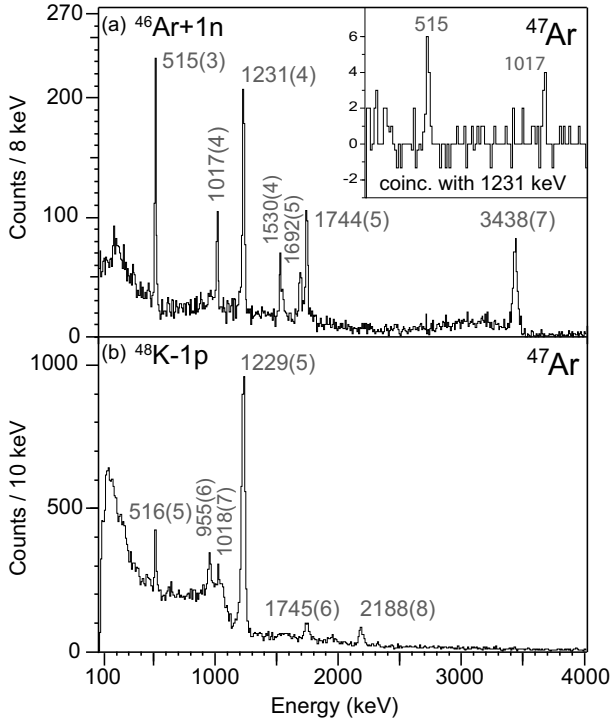

FIG. 2: Event-by-event Doppler reconstructed γ-ray spectra of ^{47}Ar: (a) as detected with GRETINA following ^{12}C(^{46}Ar,^{47}Ar+γ)X one-neutron pickup ($v/c = 0.337$) using nearest neighbor addback, and (b) one-proton removal ^{9}Be(^{48}K,^{47}Ar+γ)X with γ-ray spectroscopy using SeGA ($v/c = 0.4$). The inset to (a) shows a coincidence spectrum with a software gate applied on the 1231 keV line indicating that the 515, 1016, and 1231 keV transitions are in coincidence.

$1/2^-$ state (in both measurements) is consistent with the calculations that combine nuclear structure and reaction theory input.

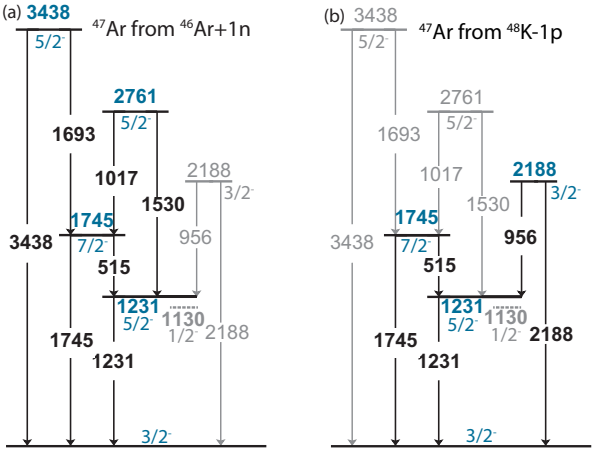

FIG. 3: (Color online) Level scheme of ^{47}Ar as observed in: (a) one-neutron pickup, and (b) one-proton removal. Levels and transitions indicated in black were observed to be populated with the respective reaction, levels and transitions marked in gray are known but were not observed in the respective reaction. The complementarity of the two reactions is apparent. Only the 1130 keV $1/2^-$ state [18] could not be accessed in the presented measurements.

The observed level scheme in the one-neutron pickup reaction is largely driven by linear and angular momentum matching conditions that favor the transfer into high-ℓ orbitals. This is quantified in Fig. 4 where the measured (Fig. 4(a)) and calculated partial cross sections, Fig. 4(b) and (c), for the population of individual bound final states are compared. The single-particle cross sections for Fig. 4(b) and (c) were calculated as summarized in Section II. Figures 4(b) and (c) only differ in the spectroscopic factors and level energies employed, using the SDPF-U [11] and SDPF-MU [10] shell-model effective interactions, respectively. The SDPF-U effective interaction describes the measured energies very well and matches the observed spectroscopic strengths pattern, at least qualitatively. The $1/2^-$ state, carrying significant $\ell = 1$ spectroscopic strength, is not expected to be populated due to orbital angular momentum mismatch reducing the single-particle cross section for pickup into the $p_{1/2}$ orbital. For the SDPF-MU effective interaction, the two strongest bound states, carrying $f_{5/2}$ strength, are lower in energy with the majority of the bound strength concentrated around 2.5 MeV, while the centroid of bound $f_{5/2}$ strength in SDPF-U is located above 3 MeV. This is indicative of a smaller $N = 32$ shell gap in SDPF-MU than in SDPF-U, with SDPF-U being closer to experiment in terms of excitation energies and single-particle strengths.

The way in which one-proton removal from odd-odd ^{48}K probes the single-particle structure is complementary to the one-neutron pickup, and more complicated.

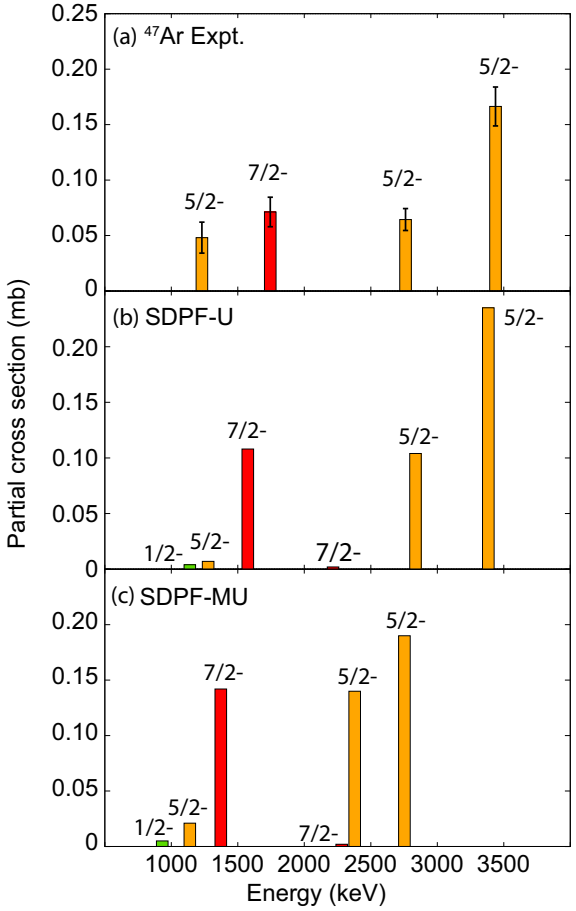

FIG. 4: (Color online) One-neutron pickup partial cross sections to excited final states: (a) as measured in the experiment, and as calculated, following Section II, with the (b) SDPF-U, and (c) SDPF-MU SM spectroscopic factors.

The ground-state spin of ^{48}K was assigned 1^- from laser-spectroscopy hyperfine structure measurements [30], confirming the earlier proposal of (1^-) by [38] from the analysis of γ-ray decay patterns in deep-inelastic transfer reactions. For the removal to a given final state of ^{47}Ar, with spin and parity J^-, typically several proton orbitals contribute. For example, non-zero $2s_{1/2}$, $1d_{3/2}$ and $1d_{5/2}$ proton spectroscopic factors characterize the wave function overlap of the ^{48}K ground state and the $^{47}\mathrm{Ar}(3/2^-_{g.s.})+p$ system (see Table I). Figure 5 compares the measured ^{9}Be(^{48}K,^{47}Ar+γ)X partial cross sections to calculations with the SDPF-U and SDPF-MU spectroscopic factors, using the formalism described in Section II. When taking into account the reduction factor of ≈ 0.5, from the one-nucleon removal systematics [24, 25] in this regime of binding ($\Delta S \approx 10.5$ MeV, Table II), the agreement between measurement and calculation is remarkable, with the SDPF-MU Hamiltonian better describing the relative populations of the $3/2^-$ and $5/2^-$ states. The most marked difference in the partial cross sections calculated with the SDPF-U and SDPF-MU SM

input is the spectroscopic strength of the first excited $3/2^-$ state at 2188 keV, where the data are closer to the SDPF-MU predictions. The overestimation of the $3/2^-_2$ partial cross section with the SDPF-U structure input can be traced back to the $2s_{1/2}$ proton spectroscopic factor that is higher by more than a factor of two as compared to SDPF-MU, and which increases the contribution to the $3/2^-$ ground state from $2s_{1/2}$ proton removal (Table I).

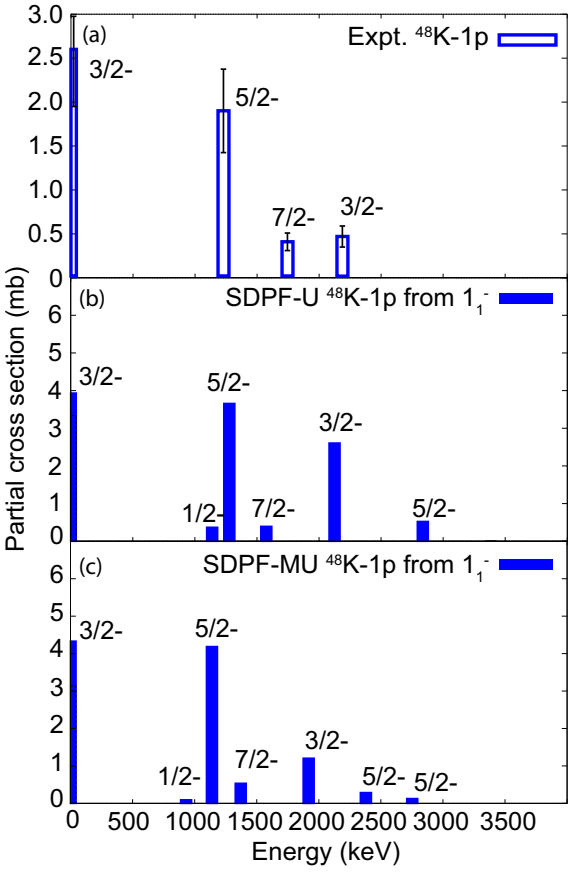

FIG. 5: (Color online) One-proton removal partial cross sections to ^{47}Ar final states: (a) as measured in the experiment, and as calculated following Section II with (b) SDPF-U, and (c) SDPF-MU shell-model spectroscopic factors. The shell-model calculations use the wave function of the lowest-lying 1^- state although this is not the ground state in either shell-model calculation. The $J^\pi = 1^-$ spin assignment was determined from laser spectroscopy [30].

Both shell-model effective interactions give a remarkably consistent picture, describing the single-particle structure of ^{47}Ar well. The SDPF-U case provides a more consistent comparison with the data in terms of the gap separating the $f_{7/2}$ orbital from the $f_{5/2}$ and the p-orbitals. On the other hand, the SDPF-MU case better describes the proton overlaps with respect to the assumed ^{48}K ground state. We note that, for both shell-model Hamiltonians, the first 1^- state is the third excited state – at 395 keV and 263 keV in SDPF-U and SDPF-MU, respectively – lying above 2^- ground and excited states in both cases.

B. First spectroscopy of ^{45}S from one-proton removal from ^{46}Cl

For the ^{9}Be(^{46}Cl,^{45}S+γ)X one-proton removal reaction, the secondary beam of ^{46}Cl (purity exceeding 98%) was produced from a 140 MeV/u stable primary beam of ^{48}Ca impinging on a 705 mg/cm^2 ^{9}Be production target at the entrance of the A1900 fragment separator [37] and separated using a 390 mg/cm^2 Al degrader. The total momentum acceptance of the A1900 was restricted to $\Delta p/p = 2\%$, yielding a rate on target of 6×10^3 ^{46}Cl/s. The 376 mg/cm^2 thick ^{9}Be reaction target was surrounded by SeGA [35] and Doppler reconstruction was performed as described for the proton removal to ^{47}Ar, discussed in Section III A. The resulting γ-ray spectrum is shown in Fig. 6. This constitutes the first observation of γ-ray transitions in the $N = 29$ nucleus ^{45}S. Given the level of statistics, $\gamma\gamma$ coincidences could not be used to build a level scheme. Instead, energy sums, intensities, and comparisons to predicted level schemes and population patterns based on SM calculations were used to propose the tentative level scheme shown as an inset in Fig. 6.

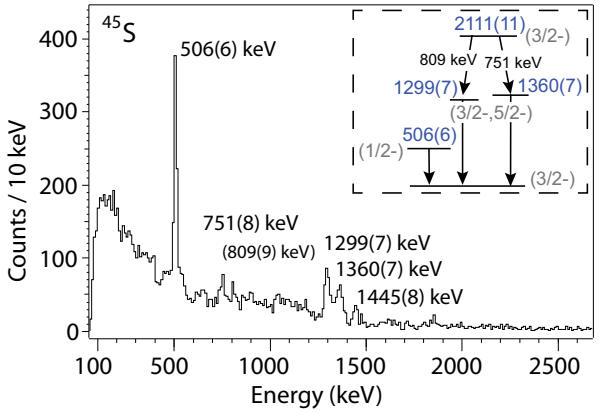

FIG. 6: (color online) Event-by-event Doppler reconstructed γ-ray spectrum of ^{45}S following population of the nucleus in the ^{9}Be(^{46}Cl,^{45}S+γ)X one-proton removal reaction ($v/c = 0.393$). The inset shows a tentative level scheme based on energy sums, intensity arguments, and comparison to shell-model calculations (see text).

A quantitative evaluation of the ^{9}Be(^{46}Cl,^{45}S+γ)X one-proton removal reaction is hardly possible since the ground-state spin of ^{46}Cl is not known. The SDPF-U and SDPF-MU Hamiltonians predict closely spaced low-lying states with $(2^-, 0^-, 1^-) = (0, 437, 480)$ keV and $(0^-, 2^-, 1^-) = (0, 162, 313)$ keV, respectively. Although not much is known about the level scheme of ^{46}Cl, the lower energy of the first excited states in SDPF-MU seems to agree better with the low-energy γ rays that

have been report from in-beam γ-ray spectroscopy [39]. Inclusive cross sections were calculated from the spectroscopic factors for both shell-model Hamiltonians, assuming each of the three spins possible for the ground state, giving $\sigma_{inc}^{-1p} = 11.8, 7.7$, and 9.2 mb for the low-lying 2^-, 1^-, and 0^- states of ^{46}Cl in SDPF-U and $\sigma_{inc}^{-1p} = 10.3, 9.3$, and 10.9 mb for the low-lying 2^-, 1^-, and 0^- states of ^{46}Cl in SDPF-MU.

As for the proton removal to ^{47}Ar, described in Section III.A, an inclusive ^{9}Be(^{46}Cl,^{45}S)X cross section of $\sigma_{inc}^{-1p} = 2.6(1)$ mb was derived from the yield of ^{45}S reaction residues divided by the number of incoming ^{46}Cl projectiles relative to the number density of the reaction target. A systematic uncertainty of 5%, attributed to the stability of the incoming beam for normalization, has been added in quadrature to the statistical uncertainty. With a reduction factor $R_s \approx 0.4$, from the systematics [24] in the binding energy regime ($\Delta S \approx 14.4$ MeV, Table III) of the ^{46}Cl projectiles, the lowest calculated inclusive cross section of 7.7 mb, for the 1^- state of ^{46}Cl within SDPF-U, agrees with the low measured inclusive cross section. Figure 7 shows the level scheme of ^{45}S as predicted by the SDPF-U shell model. There, the final state populations, from the one-proton removal reaction from the first 1^- state of ^{46}Cl, are indicated by the widths of the lines representing the levels. In comparison to the spectrum of Fig. 6, the tentative level scheme shown in the inset is conceivable. We note that both shell-model effective interactions predict an isomeric $7/2^-$ state at low energy, at 896 keV (SDPF-MU) and 746 keV (SDPF-U), with half-lives of around 500 ps and 3 ns, respectively. Should the 1^- ground-state spin suggestion be confirmed, the population of the isomeric state would account for less than 2% of the inclusive cross section within SDPF-U. The only possible indication in our spectrum for the decay of a long-lived state is a bump at about 500 keV that, in fact, appears to form the base of the strong and narrow 506 keV transition. For comparison, Fig. 3 (upper left) of Ref. [40] shows how a 336 keV τ=1.4 ns γ-ray transition would appear in a spectrum taken with SeGA in the relevant geometry and velocity regime.

A determination of the ground-state spin of ^{46}Cl would enable a more quantitative analysis, as performed for the one-proton removal from ^{48}K, and higher-statistics data would be invaluable to confirm the tentative level scheme of ^{45}S as proposed in Fig. 6.

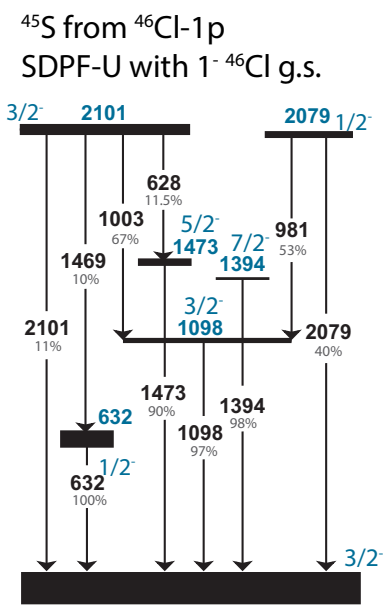

FIG. 7: (Color online) SDPF-U shell-model level scheme of ^{45}S. The widths of the lines representing energy levels are proportional to the calculated partial cross section for the ^{9}Be(^{46}Cl,^{45}S)X one-proton removal reaction, taking the wave function of the lowest 1^- state as the ground state of ^{46}Cl (see text and Table III). Only states predicted to be populated with more than 0.2 mb cross section are shown and only transitions with a branching ratio of 10% or higher are drawn.

IV. SUMMARY

We have presented a comprehensive spectroscopy of ^{47}Ar performed using two complementary direct reactions, one-neutron pickup onto ^{46}Ar projectiles and one-proton removal from the 1^- ground state of ^{48}K. Both of the state-of-the-art SDPF-U and SDPF-MU shell-model effective interactions provide a good description of the data, with (a) SDPF-U in better agreement with the ^{47}Ar excitation energies and the location of the neutron spectroscopic strength, and (b) SDPF-MU describing better the ^{47}Ar yield from proton removal from the $2s_{1/2}$ orbital in the ^{48}K ground-state. From the ^{9}Be(^{46}Cl,^{45}S+γ)X one-proton removal reaction, we report the first observed γ-ray transitions in ^{45}S. From comparisons with shell model calculations, and arguments based on intensities and energy sums, we propose a first tentative level scheme for ^{45}S. Our ^{45}S γ-ray spectrum is broadly consistent with expectations when assuming a 1^- ^{46}Cl ground-state spin and the proton spectroscopic factors from the SDPF-U interaction. Opportunities to advance our understanding of the $N = 29$ nucleus ^{45}S will emerge once the ground-state spin of ^{46}Cl is known, after which a more quantitative analysis can be performed of the one-proton removal data reported here.

Acknowledgments

GRETINA was funded by the DOE, Office of Science. Operation of the array at NSCL was supported by NSF under Cooperative Agreement PHY-1102511 (NSCL) and DOE under Grant DE-AC02-05CH11231 (LBNL). We further acknowledge support from NSF grant PHY-1404442 (NSCL), from the Department of Energy National Nuclear Security Administration under Award No. DE-NA0000979, and from the U.S. DOE, Office of Nuclear Physics, under contract DEFG02-08ER41556. D.H.

acknowledges funding from NSF grant PHY-1203100. J.A.T. acknowledges support of the Science and Technology Facilities Council (UK) grants ST/J000051 and ST/L005743.

[1] O. Sorlin, D. Guillemaud-Mueller, A. C. Mueller, V. Borrel, S. Dogny, F. Pougheon, K.-L. Kratz, H. Gabelmann, B. Pfeiffer, A. Wöhr, W. Ziegert, Yu. E. Penionzhkevich, S. M. Lukyanov, V. S. Salamatin, R. Anne, C. Borcea, L. K. Fifield, M. Lewitowicz, M. G. Saint-Laurent, D. Bazin, C. Detraz, F.-K. Thielemann, and W. Hillebrandt, Phys. Rev. C 47, 2941 (1993).

[2] H. Scheit, T. Glasmacher, B. A. Brown, J. A. Brown, P. D. Cottle, P. G. Hansen, R. Harkewicz, M. Hellström, R. W. Ibbotson, J. K. Jewell, K. W. Kemper, D. J. Morrissey, M. Steiner, P. Thirolf, and M. Thoennessen, Phys. Rev. Lett. 77, 3967 (1996).

[3] T. Glasmacher, B.A. Brown, M.J. Chromik, P.D. Cottle, M. Fauerbach, R.W. Ibbotson, K.W. Kemper, D.J. Morrissey, H. Scheit, D.W. Sklenicka, M. Steiner, Phys. Lett. B 395, 163 (1997).

[4] C. Force, S. Grevy, L. Gaudefroy, O. Sorlin, L. Caceres, F. Rotaru, J. Mrazek, N. L. Achouri, J. C. Anglique, F. Azaiez, B. Bastin, R. Borcea, A. Buta, J. M. Daugas, Z. Dlouhy, Zs. Dombradi, F. De Oliveira, F. Negoita, Y. Penionzhkevich, M. G. Saint-Laurent, D. Sohler, M. Stanoiu, I. Stefan, C. Stodel, and F. Nowacki, Phys. Rev. Lett. 105, 102501 (2010).

[5] D. Santiago-Gonzalez, I. Wiedenhöver, V. Abramkina, M. L. Avila, T. Baugher, D. Bazin, B. A. Brown, P. D. Cottle, A. Gade, T. Glasmacher, K. W. Kemper, S. McDaniel, A. Rojas, A. Ratkiewicz, R. Meharchand, E. C. Simpson, J. A. Tostevin, A. Volya, and D. Weisshaar, Phys. Rev. C 83, 061305(R) (2011).

[6] Yutaka Utsuno, Noritaka Shimizu, Takaharu Otsuka, Tooru Yoshida, and Yusuke Tsunoda, Phys. Rev. Lett. 114, 032501 (2015).

[7] J. Luis Egido, Marta Borrajo, and Tomas R. Rodriguez Phys. Rev. Lett. 116, 052502 (2016).

[8] A. Gade, P. Adrich, D. Bazin, B.A. Brown, J.M. Cook, C. Aa. Diget, T. Glasmacher, S. McDaniel, A. Ratkiewicz, K. Siwek, and D. Weisshaar, Phys. Rev. Lett. 102, 182502 (2009).

[9] B. Bastin, S. Grevy, D. Sohler, O. Sorlin, Zs. Dombradi, N. L. Achouri, J. C. Angelique, F. Azaiez, D. Baiborodin, R. Borcea, C. Bourgeois, A. Buta, A. Bürger, R. Chapman, J. C. Dalouzy, Z. Dlouhy, A. Drouard, Z. Elekes, S. Franchoo, S. Iacob, B. Laurent, M. Lazar, X. Liang, E. Lienard, J. Mrazek, L. Nalpas, F. Negoita, N. A. Orr, Y. Penionzhkevich, Zs. Podolyak, F. Pougheon, P. Roussel-Chomaz, M. G. Saint-Laurent, M. Stanoiu, and I. Stefan, Phys. Rev. Lett. 99, 022503 (2007).

[10] Yutaka Utsuno, Takaharu Otsuka, B. Alex Brown, Michio Honma, Takahiro Mizusaki, and Noritaka Shimizu, Phys. Rev. C 86, 051301(R) (2012).

[11] F. Nowacki and A. Poves, Phys. Rev. C 79, 014310 (2009).

[12] S. Takeuchi, M. Matsushita, N. Aoi, P. Doornenbal, K. Li, T. Motobayashi, H. Scheit, D. Steppenbeck, H. Wang, H. Baba, D. Bazin, L. Caceres, H. Crawford, P. Fallon, R. Gernhäuser, J. Gibelin, S. Go, S. Grevy, C. Hinke, C. R. Hoffman, R. Hughes, E. Ideguchi, D. Jenkins, N. Kobayashi, Y. Kondo, R. Krücken, T. Le Bleis, J. Lee, G. Lee, A. Matta, S. Michimasa, T. Nakamura, S. Ota, M. Petri, T. Sako, H. Sakurai, S. Shimoura, K. Steiger, K. Takahashi, M. Takechi, Y. Togano, R. Winkler, and K. Yoneda, Phys. Rev. Lett. 109, 182501 (2012).

[13] Z. Meisel, S. George, S. Ahn, J. Browne, D. Bazin, B.A. Brown, J.F. Carpino, H. Chung, R.H. Cyburt, A. Estrade, M. Famiano, A. Gade, C. Langer, M. Matos, W. Mittig, F. Montes, D.J. Morrissey, J. Pereira, H. Schatz, J. Schatz, M. Scott, D. Shapira, K. Smith, J. Stevens, W. Tan, O. Tarasov, S. Towers, K. Wimmer, J.R. Winkelbauer, J. Yurkon, and R.G.T. Zegers, Phys. Rev. Lett. 114, 022501 (2015).

[14] A. Gade, D. Bazin, C. M. Campbell, J. A. Church, D. C. Dinca, J. Enders, T. Glasmacher, Z. Hu, K. W. Kemper, W. F. Mueller, H. Olliver, B. C. Perry, L. A. Riley, B. T. Roeder, B. M. Sherrill, and J. R. Terry Phys. Rev. C 68, 014302 (2003).

[15] R. Winkler, A. Gade, T. Baugher, D. Bazin, B. A. Brown, T. Glasmacher, G. F. Grinyer, R. Meharchand, S. McDaniel, A. Ratkiewicz, and D. Weisshaar, Phys. Rev. Lett. 108, 182501 (2012).

[16] S. Calinescu et al., Acta Phys. Pol. B 45, 199 (2014).

[17] D. Mengoni, J. J. Valiente-Dobon, A. Gadea, S. Lunardi, S. M. Lenzi, R. Broda, A. Dewald, T. Pissulla, L. J. Angus, S. Aydin, D. Bazzacco, G. Benzoni, P. G. Bizzeti, A. M. Bizzeti-Sona, P. Boutachkov, L. Corradi, F. Crespi, G. de Angelis, E. Farnea, E. Fioretto, A. Goergen, M. Gorska, A. Gottardo, E. Grodner, A. M. Howard, W. Krolas, S. Leoni, P. Mason, D. Montanari, G. Montagnoli, D. R. Napoli, A. Obertelli, R. Orlandi, T. Pawlat, G. Pollarolo, F. Recchia, A. Algora, B. Rubio, E. Sahin, F. Scarlassara, R. Silvestri, J. F. Smith, A. M. Stefanini, D. Steppenbeck, S. Szilner, C. A. Ur, P. T. Wady, and J. Wrzesinski, Phys. Rev. C 82, 024308 (2010).

[18] L. Gaudefroy, O. Sorlin, D. Beaumel, Y. Blumenfeld, Z. Dombradi, S. Fortier, S. Franchoo, M. Gelin, J. Gibelin, S. Grevy, F. Hammache, F. Ibrahim, K.W. Kemper, K.-L. Kratz, S.M. Lukyanov, C. Monrozeau, L. Nalpas, F. Nowacki, A.N. Ostrowski, T. Otsuka, Yu.-E. Penionzhkevich, J. Piekarewicz, E.C. Pollacco, P. Roussel-Chomaz, E. Rich, J.A. Scarpaci, M.G. St.Laurent, D. Sohler, M. Stanoiu, T. Suzuki, E. Tryggestad, D. Verney, Phys. Rev. Lett. 97, 092501 (2006).

[19] S. Bhattacharyya, M. Rejmund, A. Navin, E. Caurier, F. Nowacki, A. Poves, R. Chapman, D. O'Donnell, M. Gelin, A. Hodsdon, X. Liang, W. Mittig, G. Mukherjee, F. Rejmund, M. Rousseau, P. Roussel-Chomaz, K.-M. Spohr, Ch. Theisen, Phys. Rev. Lett. 101, 032501 (2008).

[20] D. Steppenbeck, S. Takeuchi, N. Aoi, P. Doornenbal, M. Matsushita, H. Wang, Y. Utsuno, H. Baba, S. Go, J. Lee, K. Matsui, S. Michimasa, T. Motobayashi, D. Nishimura, T. Otsuka, H. Sakurai, Y. Shiga, N. Shimizu, P.-A. Soderstrom, T. Sumikama, R. Taniuchi, J.J. Valiente-Dobon, K. Yoneda, Phys. Rev. Lett. 114, 252501 (2015).

[21] NuShellX, http://www.garsington.eclipse.co.uk/

[22] S. Takeuchi *et al.*, Phys. Rev. Lett. 109, 182501 (2012).

[23] P. G. Hansen and J. A. Tostevin, Annu. Rev. Nucl. Part. Sci. 53, 219 (2003).

[24] J. A. Tostevin and A. Gade, Phys. Rev. C 90, 057602 (2014).

[25] A. Gade, P. Adrich, D. Bazin, M. D. Bowen, B. A. Brown, C. M. Campbell, J. M. Cook, T. Glasmacher, P. G. Hansen, K. Hosier, S. McDaniel, D. McGlinchery, A. Obertelli, K. Siwek, L. A. Riley, J.A. Tostevin, and D. Weisshaar, Phys. Rev. C 77, 044306 (2008).

[26] B. A. Brown, Phys. Rev. C 58, 220 (1998).

[27] J. A. Tostevin, G. Podolyak, B. A. Brown, and P. G. Hansen, Phys. Rev. C 70, 064602 (2004); J. A. Tostevin and B. A. Brown, ibid. 74, 064604 (2006).

[28] L. Ray, Phys. Rev. C 20, 1857 (1979).

[29] M. Wang, G. Audi, A. H. Wapstra, F. G. Kondev, M. MacCormick, X. Xu, and B. Pfeiffer, Chin. Phys. C 36, 1603 (2012).

[30] K. Kreim, M.L. Bissell, J. Papuga, K. Blaum, M. De Rydt, R.F. Garcia Ruiz, S. Goriely, H. Heylen, M. Kowalska, R. Neugart, G. Neyens, W. Nörtershäuser, M.M. Rajabali, R. Sanchez Alarcon, H.H. Stroke, D.T. Yordanov, Phys. Lett. B 731, 97 (2014).

[31] A. Gade, J. A. Tostevin, V. Bader, T. Baugher, D. Bazin, J. S. Berryman, B. A. Brown, D. J. Hartley, E. Lunderberg, F. Recchia, S. R. Stroberg, Y. Utsuno, D. Weisshaar, and K. Wimmer, Phys. Rev. C 93, 031601(R) (2016).

[32] Supplement to [31].

[33] G. van der Steenhoven, H. P. Blok, E. Jans, M. de Jong, L. Lapikas, E. N. M. Quint and P. K. A. de Witt Huberts, Nucl. Phys. A480, 547 (1988).

[34] D. Bazin *et al.*, Nucl. Instrum. Methods Phys. Res., Sect. B 204, 629 (2003).

[35] W. F. Mueller *et al.*, Nucl. Instrum. Methods Phys. Res., Sect. A 466, 492 (2001).

[36] S. Paschalis, I.Y. Lee, A.O. Macchiavelli, C.M. Campbell, M. Cromaz, S. Gros, J. Pavan, J. Qian, R.M. Clark, H.L. Crawford, D. Doering, P. Fallon, C. Lionberger, T. Loew, M. Petri, T. Stezelberger, S. Zimmermann, D.C. Radford, K. Lagergren, D. Weisshaar, R. Winkler, T. Glasmacher, J.T. Anderson, C.W. Beausang, Nucl. Instrum. Methods Phys. Res., Sect. A 709, 44 (2013).

[37] D. J. Morrissey *et al.*, Nucl. Instrum. Methods Phys. Res., Sect. B 204, 90 (2003).

[38] W. Krolas, R. Broda, B. Fornal, R. V. F. Janssens, A. Gadea, S. Lunardi, J. J. Valiente-Dobon, D. Mengoni, N. Marginean, L. Corradi, A. M. Stefanini, D. Bazzacco, M. P. Carpenter, G. De Angelis, E. Farnea, E. Fioretto, F. Galtarossa, T. Lauritsen, G. Montagnoli, D. R. Napoli, R. Orlandi, T. Pawlat, I. Pokrovskiy, G. Pollarolo, E. Sahin, F. Scarlassara, D. Seweryniak, S. Szilner, B. Szpak, C. A. Ur, J. Wrzesinski, and S. Zhu, Phys. Rev. C 84, 064301 (2011).

[39] S. R. Stroberg, A. Gade, T. Baugher, D. Bazin, B. A. Brown, J. M. Cook, T. Glasmacher, G. F. Grinyer, S. McDaniel, A. Ratkiewicz, and D. Weisshaar, Phys. Rev. C 86, 024321 (2012).

[40] J. R. Terry, B. A. Brown, C. M. Campbell, J. M. Cook, A. D. Davies, D.-C. Dinca, A. Gade, T. Glasmacher, P. G. Hansen, B. M. Sherrill, H. Zwahlen, D. Bazin, K. Yoneda, J. A. Tostevin, T. Otsuka, Y. Utsuno, and B. Pritychenko, Phys. Rev. C 77, 014316 (2008).